ACS OMEGA

http://pubs.acs.org/journal/acsodf

Article

Terahertz Spectroscopy and DFT Analysis of Phonon Dynamics of the Layered Van der Waals Semiconductor Nb_3X_8 (X = Cl, I)

Jangwon Kim, Youjin Lee, Young Woo Choi, Taek Sun Jung, Suhan Son, Jonghyeon Kim, Hyoung Joon Choi,* Je-Geun Park,* and Jae Hoon Kim*

Cite This: *ACS Omega* 2023, 8, 14190−14196

Read Online

ACCESS | Metrics & More | Article Recommendations | Supporting Information

ABSTRACT: We have conducted a terahertz spectroscopic study and a density functional theory analysis of the phonon dynamics of the layered van der Waals semiconductors Nb_3Cl_8 and Nb_3I_8. Several infrared-active phonon modes were observed in the terahertz region, and their frequencies were found to be in excellent agreement with our first-principles lattice dynamics calculations. For Nb_3Cl_8, the observed phonon spectra are consistent with a structural transition at 90 K from the high-temperature $P\bar{3}m1$ phase to the low-temperature $R\bar{3}m$ phase. Also, our study confirmed that the structural and magnetic transitions were coupled in Nb_3Cl_8. For Nb_3I_8, which is nonmagnetic at and below room temperature, no significant temperature or magnetic field dependence was observed in the phonon spectra. Our study provides an intriguing connection between the structural properties and the paramagnetic−nonmagnetic transitions in Nb_3Cl_8 and Nb_3I_8.

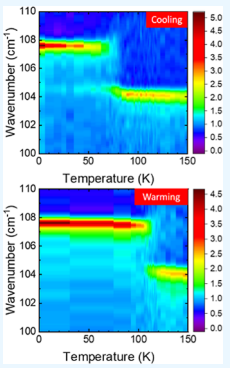

INTRODUCTION

The discovery of graphene and its extremely high mobility has paved the way for research on two-dimensional (2D) materials.[1] However, the absence of a band gap in graphene limits its applicability in electronic devices. Various alternative 2D materials with sizeable band gaps have been investigated, including black phosphorus,[2] transition-metal dichalcogenides,[3] and hexagonal boron nitride.[4] The majority of these 2D materials possess atomic layers bonded by van der Waals (vdW) forces and can be exfoliated down to the monolayer, thereby displaying exotic physical properties such as the valley degree of freedom,[5] topological band structure,[6] and pseudospin polarization.[7] Magnetic vdW materials exhibiting 2D magnetism in the monolayer or bilayer limit have recently emerged.[8] Among these, CrI_3,[9] $Cr_2Ge_2Te_6$,[10] and Fe_3GeTe_2[11] were observed to exhibit ferromagnetic order, whereas $NiPS_3$[12] and $FePS_3$[13] exhibit antiferromagnetic order. Many of these novel magnetic materials have attracted much attention owing to their potential applications in quantum memory and spintronic devices.

In contrast to vdW magnetic materials containing magnetic elements, a closely related class of vdW materials without magnetic elements, such as Nb_3Cl_8, Nb_3Br_8, and Nb_3I_8, have been investigated in connection with possible cluster magnetism.[14] Bulk Nb_3Cl_8 and Nb_3Br_8 were observed to be in a paramagnetic state at high temperatures and in a nonmagnetic singlet state at low temperatures.[15,16] Indeed, these materials have been confirmed to exhibit paramagnetic−nonmagnetic transitions at 92 and 382 K, respectively,[16] whereas Nb_3I_8 is expected to undergo a similar transition at a much higher temperature. Density functional theory (DFT) calculations based on a mean-field approximation of the classical Heisenberg model predicted that a monolayer in Nb_3X_8 (where X = Cl, Br, and I) should possess a ferromagnetic ground state with semiconducting properties; however, this is yet to be confirmed experimentally.[17]

Despite these peculiar characteristics, little fundamental experimental research has been conducted on Nb_3X_8 (where X = Cl, Br, and I) until recently. This class of materials have a common structure of a trimerized kagome lattice with three Nb atoms forming a triangular cluster with a net effective spin S_{eff} = 1/2.[16] The band gaps of Nb_3Cl_8 and Nb_3I_8 were experimentally reported to be 1.12 and ∼1 eV, respectively,[18,19] thereby indicating their potential in device applications. Additionally, Nb_3Cl_8 and Nb_3I_8 have been experimentally confirmed to possess topological flat bands.[18,20]

In this paper, we report on our terahertz spectroscopic study and DFT analysis of the phonon dynamics of Nb_3Cl_8 and Nb_3I_8 in the spectral range of 5−125 cm^{-1} (0.6−15.5 meV), in the temperature range of 1.5−300 K, and in the magnetic field range of 0−7 T. Several sharp absorption peaks corresponding to infrared-active optical phonon modes were observed, with their frequency positions in excellent agreement with our DFT

Received: February 15, 2023
Accepted: March 28, 2023
Published: April 8, 2023

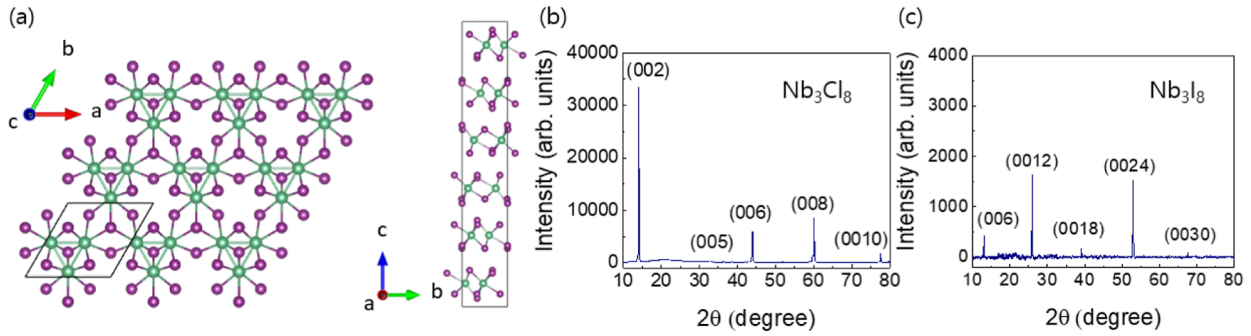

Figure 1. (a) Crystal structure ($P\bar{3}m1$) of Nb_3X_8 (X = Cl, I). Nb (green) atoms form a trimerized kagome lattice. Six X (purple) atoms are bonded to a single Nb atom in a distorted octahedral structure. The rhombus indicates the unit cell. XRD of (b) bulk Nb_3Cl_8 and (c) bulk Nb_3I_8.

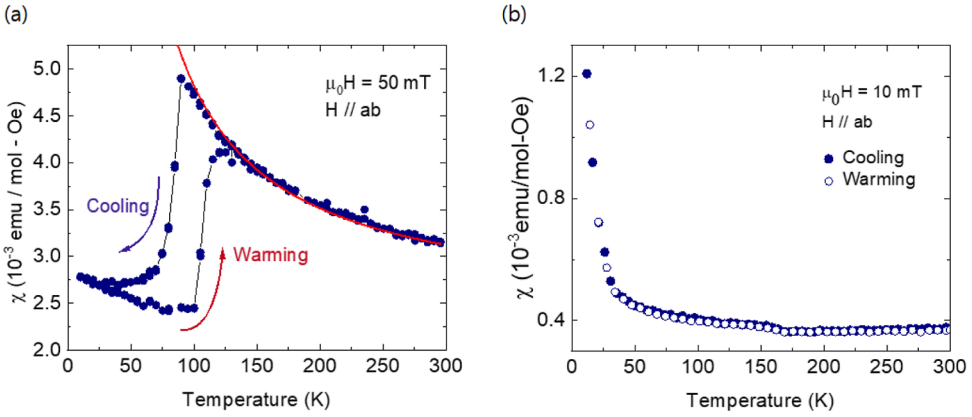

Figure 2. Temperature-dependent magnetic susceptibility of bulk single crystals (a) Nb_3Cl_8 and (b) Nb_3I_8. Nb_3Cl_8 has a magnetic transition from a paramagnetic phase to a non-magnetic phase at 90 K, but Nb_3I_8 does not show a magnetic phase transition below 300 K. The samples have been field-cooled (FC) under a small magnetic field of μ_0H = 50 mT for Nb_3Cl_8 and 10 mT for Nb_3I_8 along the ab plane. The solid red line is a Curie–Weiss fit for the paramagnetic state.

lattice dynamics calculations. Additionally, notable changes in the phonon absorption spectra were observed across the magnetic–structural phase transition at 90 K in Nb_3Cl_8. Our results provide new information on the fundamental properties of the layered vdW semiconductors in the Nb_3X_8 family and are expected to open a new avenue for research on similar materials.

EXPERIMENTAL METHODS

Crystal Growth and Characterization. Nb_3Cl_8 and Nb_3I_8 single crystals were synthesized by using the chemical vapor transport method. To prepare Nb_3Cl_8, Nb powder (Alfa Aesar, 99.99%) and $NbCl_5$ (Alfa Aesar, 99.95%) were mixed stoichiometrically with NH_4Cl (Alfa Aesar 99.999%) as the transport agent.[16] For Nb_3I_8, Nb powder (Alfa Aesar, 99.99%) and iodine powder (Alfa Aesar, 99.99%) were mixed stoichiometrically with excess iodine. The powder mixtures were sealed in a quartz tube cylinder and placed in a two-zone furnace. The temperature gradients were 840 to 795 °C for Nb_3Cl_8 and 650 to 620 °C for Nb_3I_8. This temperature condition was kept for 3 days. To check the sample quality and crystallinity, powder X-ray diffraction (XRD) measurements were performed (Miniflex II, Rigaku).

Magnetic Susceptibility. The magnetic susceptibilities of the Nb_3Cl_8 and Nb_3I_8 crystals were measured by using commercial magnetometers (MPMS-3 and MPSM-XL5, Quantum Design). Temperature-dependent magnetic susceptibility data of Nb_3Cl_8 and Nb_3I_8 were measured under a weak external field of H = 50 mT (500 Oe) for Nb_3Cl_8 and 10 mT (100 Oe) for Nb_3I_8 along the ab plane.

Terahertz Time-Domain Spectroscopy. Terahertz time-domain spectroscopy was performed over the spectral range of 5 to 125 cm^{-1} (0.62–15.5 meV) by using a terahertz time-domain spectrometer (TERA K15, Menlo Systems). Prior to the terahertz experiment, Nb_3Cl_8 and Nb_3I_8 crystals were thinned down to approximately 20 and 80 μm (as measured by a micrometer), respectively, by using Scotch tape. To observe the temperature and magnetic field dependences, transmission measurements were performed over the temperature range of 1.5–300 K and in the magnetic field range of 0–7 T by using a helium-free magneto-optic cryostat (SpectromagPT, Oxford Instruments). The entire optical path was kept under nitrogen purge to remove water-vapor absorption in the ambient atmosphere.

DFT Lattice Dynamics Calculations. We performed first-principles DFT lattice dynamics calculations using the Quantum ESPRESSO package.[21] We used the norm-conserving pseudopotentials from the Pseudo-Dojo library,[22] with the electron wavefunction cutoff of 90 Ry and a 5 × 5 × 5 and 8 × 8 × 4 k-point grid for the Brillouin zone integration over the unit cells of the $R\bar{3}m$ and $P\bar{3}m1$ phases, respectively. The exchange–correlation energy is approximated by the rVV10 functional,[23] which includes the non-local vdW interaction energy. The atomic positions were relaxed until the atomic forces on each atom were below 0.001 eV/Å. The Γ-point phonon frequencies were calculated via density functional perturbation theory (DFPT).[24] Assuming the ab

https://doi.org/10.1021/acsomega.3c01019
ACS Omega 2023, 8, 14190−14196

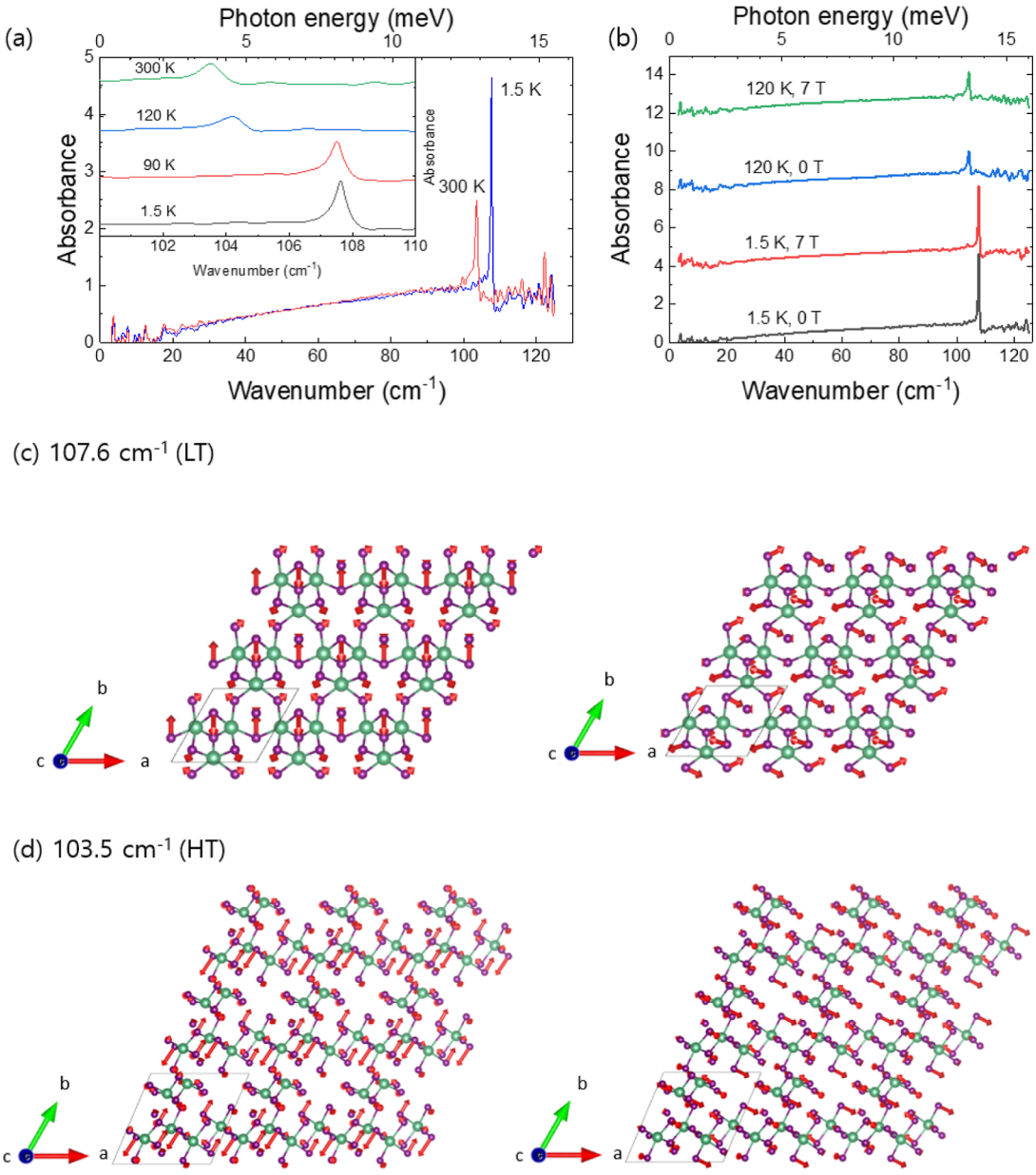

Figure 3. (a) Temperature-dependent *ab*-plane absorbance spectra of single-crystal Nb_3Cl_8. The only phonon mode of Nb_3Cl_8 observed in our terahertz range of measurement has an energy of 107.6 cm^{-1} at 1.5 K and 103.5 cm^{-1} at 300 K. Absorption spectra at various temperatures are shown in the inset. The magnetic field dependence of this single mode is shown in (b) at 1.5 and 120 K (spectra were systematically shifted vertically for clarity). The atomic displacements of the single mode in Nb_3Cl_8 are shown at (c) low-temperature (LT, $R\bar{3}m$) and (d) high-temperature (HT, $P\bar{3}m1$) phases. Nb and Cl atoms are represented by green and purple spheres, respectively. As the a and *b* directions (in-plane) are equivalent due to crystal symmetry, both degenerate modes are shown.

plane polarized light, the infrared (IR) activity of a phonon mode ν is calculated as IR = $I_{\nu,x}^2 + I_{\nu,y}^2$, where $I_{\nu,\alpha} = \sum_\beta Z_{\kappa,\alpha\beta}^* u_{\nu,\kappa\beta}$, $Z_{\kappa,\alpha\beta}^*$ is the Born effective charge tensor and $u_{\nu,\kappa\beta}$ is the α-th component of the phonon eigenvector for atom κ.

RESULTS AND DISCUSSION

Figure 1 shows the crystal structure ($P\bar{3}m1$) of Nb_3X_8 (X = Cl, I) at room temperature. The space group of bulk Nb_3Cl_8 is $P\bar{3}m1$ at room temperature, but its low-temperature structure, possibly $R\bar{3}m$, has not been clearly identified. For Nb_3I_8, the space group is $R\bar{3}m$ at and below room temperature.[25] The unit cell of Nb_3X_8 (Figure 1a) contains three Nb atoms and eight halide atoms. In bulk Nb_3X_8, 2D layers (the *ab* plane) are stacked along the *c* axis, and individual layers are bonded via weak vdW interactions. The three nearest Nb atoms form a triangular trimer cluster with strong metallic bonds. Overall, there are two types of Nb bondings of different lengths: the intracluster distance is 2.81 Å, and the intercluster distance is 3.93 Å.[15] Thus, each atomic plane of this layered structure constitutes a trimerized (breathing) kagome lattice, as shown in Figure 1a. Each Nb atom is surrounded by six halide atoms, forming a distorted octahedron. The single-crystal Nb_3Cl_8 and Nb_3I_8(001) peaks in powder XRD (Figure 1b,c, respectively) are consistent with the reported lattice parameters; c = 12.268 Å for Nb_3Cl_8,[26] and c = 41.715 Å for Nb_3I_8.[27] The XRD measurement was performed under the condition of the

https://doi.org/10.1021/acsomega.3c01019
ACS Omega 2023, 8, 14190−14196

Table 1. Calculated Optical Phonon Modes of Nb_3Cl_8 in Our Terahertz Measurement Range[a]

$R\bar{3}m$ phase			$P\bar{3}m1$ phase		
frequency (cm^{-1})	Irrep. (degeneracy)	type	frequency (cm^{-1})	Irrep. (degeneracy)	type
21.96	E_g (2)	R	28.06	E_g (2)	R
65.17	A_{1g} (1)	R	61.31	A_{1g} (1)	R
104.2	E_u (2)	IR	97.87	E_g (2)	R
106.22	E_g (2)	R	99.45	E_u (2)	IR
109.45	A_{2g} (1)	R	107.7	A_{2g} (1)	R
113.51	A_{1u} (1)	R	112.16	A_{1u} (1)	R
120.03	E_g (2)	R	118.86	E_g (2)	R

[a]IR and R indicate infrared- and Raman-active modes, respectively. Irrep. means irreducible representations. The number within the parentheses indicates degeneracy. For both phases, only twofold degenerate E_u modes are IR active below 125 cm^{-1}.

scattering vector being parallel to (00*l*). In this restricted condition, only (00*l*) diffraction peaks were observed, indicating the high quality of our as-grown crystals.

The magnetic susceptibilities of Nb_3Cl_8 and Nb_3I_8 were measured by using commercial magnetometers (MPMS-3 and MPSM-XL5, Quantum Design). Figure 2a,b shows the temperature dependences of the magnetic susceptibilities of Nb_3Cl_8 and Nb_3I_8 single crystals over the temperature range of 2−300 K, measured under a weak external magnetic field of $\mu_0 H$ = 50 mT for Nb_3Cl_8 and 10 mT for Nb_3I_8 along the *ab* plane. From the Curie−Weiss fitting for Nb_3Cl_8 (red solid line), the Curie constant and temperature are evaluated as C = 0.206 emu K/mol Oe (μ_{eff} = 1.28 μ_0, where μ_0 is the Bohr magneton) and θ_{CW} = 15 K, respectively. Our measurement results confirm that Nb_3Cl_8 undergoes a paramagnetic−nonmagnetic transition at T_c = 90 K. The magnetic susceptibility was strongly suppressed below 90 K for Nb_3Cl_8 and over the entire temperature range of 2−300 K for Nb_3I_8 (Figure 2). The strongly suppressed and temperature-independent magnetic susceptibility indicates the non-magnetic phase at low temperatures, except for the possible presence of magnetic impurities visible in the Curie-like tails at the lowest temperature of our measurement. Therefore, Nb_3Cl_8 and Nb_3I_8 possess a nonmagnetic state below 90 and 300 K, respectively, which is consistent with the singlet state of Nb trimers. Additionally, the value of T_c for Nb_3I_8 is likely to be even higher than that of Nb_3Br_8 (T_c = 382 K).[16]

Our terahertz transmission measurements were performed over the frequency range of 5−125 cm^{-1} and in the temperature range of 1.5−300 K. Figure 3a shows the absorption spectra of an approximately 30 μm thick single crystal of Nb_3Cl_8 at 1.5 and 300 K. Nb_3Cl_8 exhibited a single phonon mode with energy at 107.6 cm^{-1} at 1.5 K and 103.5 cm^{-1} at 300 K. The inset in Figure 3a shows the absorption spectra at several different temperatures. In the low temperature (LT) phase below 90 K, the energy of this phonon mode barely changed from 107.6 cm^{-1} at 1.5 K to 107.5 cm^{-1} at 90 K. Likewise, in the high temperature (HT) phase above 90 K, the phonon mode barely changed from 104.2 cm^{-1} at 120 K to 103.5 cm^{-1} at 300 K. The sudden frequency shift in this phonon mode occurs because Nb_3Cl_8 undergoes a structural phase transition at 90 K, with its symmetry changing from $P\bar{3}m1$ at high temperatures to $R\bar{3}m$ at low temperatures. There is indeed some controversy on the assignment of the latter structure for low temperatures.[14−16] On the other hand, these peaks were not responsive to magnetic fields up to 7 T (Figure 3b). Figure 3c,d indicates the atomic displacements of the lowest infrared (IR) active optical modes (E_u symmetry) (twofold degenerate) found in our DFT lattice dynamics calculations. In both modes, Nb atoms exhibit relatively small displacements, and the out-of-phase motion of two of the six Cl atoms surrounding each Nb atom dominates the vibration

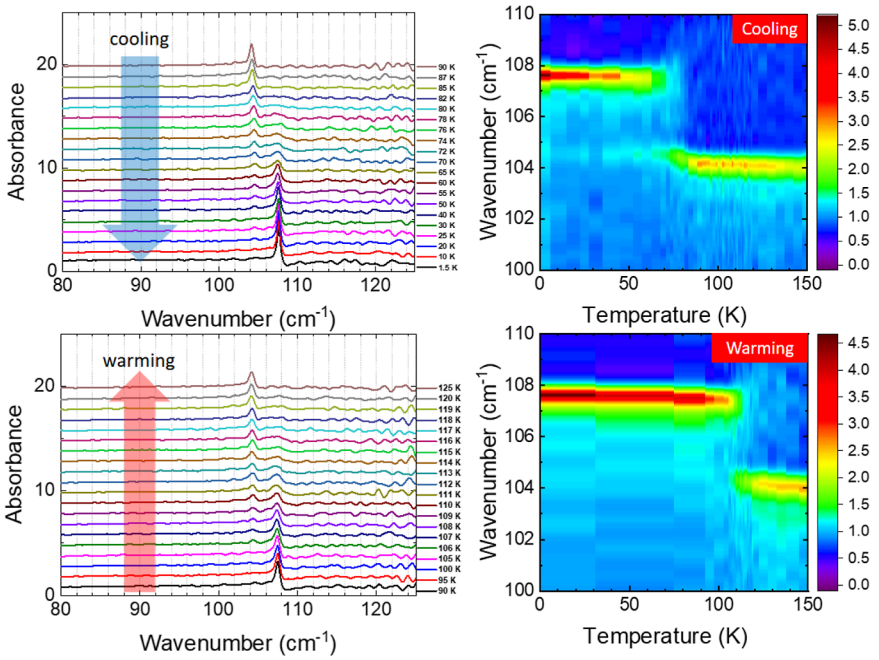

Figure 4. Temperature-dependent *ab*-plane absorbance spectra of single crystal Nb_3Cl_8 around the paramagnetic to the non-magnetic phase transition at 90 K. Spectra were systematically shifted vertically for clarity. Nb_3Cl_8 appears to go through a phase transition at about 80 K as the sample is cooled and at about 110 K as the sample is heated. Color scale bars represent the absorbance intensities.

https://doi.org/10.1021/acsomega.3c01019
ACS Omega 2023, 8, 14190−14196

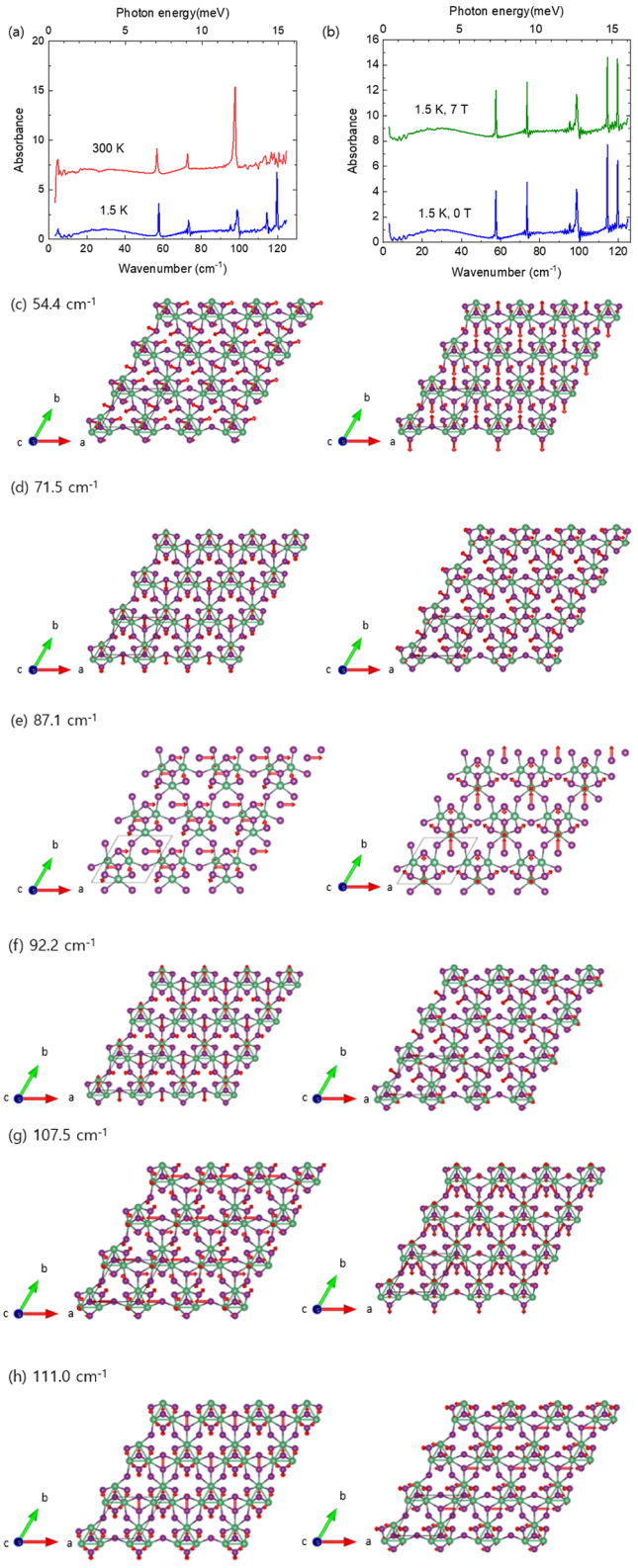

Figure 5. (a) Temperature-dependent *ab*-plane absorption spectra of single-crystal Nb_3I_8. Because Nb_3I_8 exhibits no phase transition at or below 300 K, no significant change in the phonon energies was observed. (b) Magnetic field-dependence of the absorption spectrum at 1.5 K in Nb_3I_8. The peaks are not responsive to a magnetic field. For (a,b), spectra were systematically shifted vertically for clarity. (c–h) The atomic displacements of twofold degenerate E_u phonon modes of Nb_3I_8.

Table 2. Calculated Optical Phonon Modes of Nb_3I_8 in Our Terahertz Measurement Range[a]

frequency (cm^{-1})	Irrep. (degeneracy)	type	intensity
21.95	E_g (2)	R	
45.13	A_{1g} (1)	R	
54.75	E_u (2)	IR	0.131
55.84	E_g (2)	R	
63.47	E_g (2)	R	
68.70	A_{2g} (1)	R	
71.89	E_u (2)	IR	0.070
73.70	A_{1u} (1)	R	
84.21	E_g (2)	R	
87.31	E_u (2)	IR	0.002
88.49	A_{2u} (1)	IR	
90.23	A_{1g} (1)	R	
92.39	E_u (2)	IR	0.440
92.41	E_g (2)	R	
94.00	A_{1g} (1)	R	
94.44	A_{2g} (1)	R	
96.29	A_{1u} (1)	R	
97.43	A_{2u} (1)	IR	
106.38	A_{1g} (1)	R	
106.81	A_{2u} (1)	IR	
107.02	E_g (2)	R	
107.54	E_u (2)	IR	0.126
111.18	E_u (2)	IR	0.017
111.26	E_g (2)	R	
122.89	A_{2u} (1)	IR	
125.50	A_{1g} (1)	R	

[a]The labels are the same as in Table 1. The A_{2u} and E_u modes are out-of-plane and in-plane vibrations, respectively. Intensity refers to the oscillator strength of the in-plane IR-active modes.

pattern. Also, the motion of the corresponding mode in the HT phase is qualitatively very similar to that in the LT phase.

Table 1 shows the calculated optical phonon modes of Nb_3Cl_8 in $R\bar{3}m$ and $P\bar{3}m1$ phases, respectively. We find that only a twofold degenerate E_u mode is infrared (IR)-active below 125 cm^{-1} for both phases. The atomic displacements of this E_u mode consist mostly of in-plane vibrations of Cl atoms (Figure 3c,d). Since this E_u mode is the only IR active mode in our terahertz measurement range, we believe that the E_u mode of the $R\bar{3}m$ ($P\bar{3}m1$) phase accounts for the experimental IR peak of the low (high) temperature phase at 107.6 cm^{-1} (103.5 cm^{-1}). Although the calculated frequencies are slightly underestimated due to a systematic error in DFT, we find excellent agreement between experiment and theory for the difference in IR active phonon frequencies in the two phases.

Additionally, our experiment shows that the structural and magnetic phase transitions can be tracked by observing a shift in the phonon vibrational energy in Nb_3Cl_8. To determine an accurate structural phase transition temperature, the temperature dependence in the terahertz absorption spectra was studied in more detail. Figure 4 shows the absorbance spectra around the structural phase transition temperature. A rather sudden jump in the frequency position has been spotted at approximately 80 K during cooling and at 110 K during warming. Compared to magnetic susceptibility (Figure 2), we conclude that the structural and magnetic phase transitions occur simultaneously (Figure S1). Indeed, these results pinpoint a subtle connection between the structural phase transition and the magnetic phase transition in Nb_3Cl_8.

https://doi.org/10.1021/acsomega.3c01019
ACS Omega 2023, 8, 14190−14196

The absorbance spectra of Nb_3I_8 in Figure 5a show phonon absorption peaks at 57.7, 73.3, 95.3, 98.7, 114.3, and 119.7 cm^{-1} at 1.5 K (Figure 5a). The atomic displacements are presented in Figure 5c−h. For these six modes, we find good agreement between experiment and theory. Unlike in Nb_3Cl_8, abrupt phonon energy shifts were not observed in Nb_3I_8 owing to the absence of a structural or magnetic phase transition below 300 K. The absorption peaks were unresponsive to magnetic field up to 7 T (Figure 5b), and their energies were consistent with the calculated energies of E_u phonon modes (Table 2) within our terahertz measurement range.

Table 2 shows the calculated optical phonon modes of Nb_3I_8 in $R\bar{3}m$ phase. The total number of IR active phonon modes is the same for two materials. However, in our experimental measurement range, which is below 125 cm^{-1}, the phonon modes of Nb_3Cl_8 and Nb_3I_8 are dominantly from Cl and I atomic vibrations, respectively. Since heavier atoms result in lower phonon frequencies, Nb_3I_8 has more IR-active phonon modes that fall into our experimental measurement range, while Nb_3Cl_8 has only one IR-active mode in that range. The A_{2u} and E_u modes are out-of-plane and in-plane vibrations, respectively. In addition, our DFPT calculations show that the E_u mode at 87.31 cm^{-1} has negligible IR activity. The frequencies of the remaining 5 E_u modes are in good agreement with the peak positions measured in our terahertz spectroscopy experiments. Figure 5c−h shows the calculated atomic displacements of E_u modes that have non-negligible in-plane IR activity.

CONCLUSIONS

We investigated the phonon dynamics of the layered vdW semiconductors Nb_3Cl_8 and Nb_3I_8 by performing terahertz time-domain spectroscopy and analyzing the frequency, temperature, and magnetic field dependences based on DFT calculations. No remarkable changes in the phonon spectra were found in the case of Nb_3I_8, which does not exhibit a paramagnetic−nonmagnetic transition below room temperature. In the case of Nb_3Cl_8, a substantial change in an E_u infrared-active phonon mode was found in accordance with the paramagnetic−nonmagnetic transition at 90 K, which supports the assignment of the $R\bar{3}m$ space group for the low-temperature phase of Nb_3Cl_8. Our results elucidate a detailed connection between the lattice dynamics and the paramagnetic−nonmagnetic transition in this important family of layered vdW semiconductors.

ASSOCIATED CONTENT

Data Availability Statement

The data that support the findings of this study are available from the corresponding author upon reasonable request.

Supporting Information

The Supporting Information is available free of charge at https://pubs.acs.org/doi/10.1021/acsomega.3c01019.

Temperature-dependent intensity of the low- and high-temperature phonon modes of Nb_3Cl_8 (PDF)

AUTHOR INFORMATION

Corresponding Authors

Hyoung Joon Choi − *Department of Physics, Yonsei University, Seoul 03722, Republic of Korea;* orcid.org/0000-0001-8565-8597; Email: h.j.choi@yonsei.ac.kr

Je-Geun Park − *Center for Quantum Materials and Department of Physics and Astronomy & Institute of Applied Physics, Seoul National University, Seoul 08826, Republic of Korea;* orcid.org/0000-0002-3930-4226; Email: jgpark10@snu.ac.kr

Jae Hoon Kim − *Department of Physics, Yonsei University, Seoul 03722, Republic of Korea;* orcid.org/0000-0002-7840-3630; Email: super@yonsei.ac.kr

Authors

Jangwon Kim − *Department of Physics, Yonsei University, Seoul 03722, Republic of Korea*

Youjin Lee − *Center for Quantum Materials and Department of Physics and Astronomy & Institute of Applied Physics, Seoul National University, Seoul 08826, Republic of Korea*

Young Woo Choi − *Department of Physics, Yonsei University, Seoul 03722, Republic of Korea;* Present Address: Department of Physics, University of California, Berkeley, California 94720, USA; orcid.org/0000-0003-4725-1299

Taek Sun Jung − *Department of Physics, Yonsei University, Seoul 03722, Republic of Korea;* orcid.org/0000-0002-0847-6746

Suhan Son − *Center for Quantum Materials and Department of Physics and Astronomy & Institute of Applied Physics, Seoul National University, Seoul 08826, Republic of Korea;* Present Address: Department of Physics, University of Michigan, Ann Arbor, MI 48109, USA.

Jonghyeon Kim − *Department of Physics, Yonsei University, Seoul 03722, Republic of Korea*

Complete contact information is available at: https://pubs.acs.org/10.1021/acsomega.3c01019

Author Contributions

J.K., Y.L., and Y.W.C. contributed equally to this work. J.H.K., J.-G.P., and H.J.C. supervised the project. The samples were synthesized and characterized by Y.L. and S.S. Time-domain terahertz spectroscopy was performed by J.K., T.S.J., J.K., and J.H.K. discussed the terahertz experiments. The theoretical calculations were performed by Y.W.C. All authors participated in writing the manuscript.

Notes

The authors declare no competing financial interest.

ACKNOWLEDGMENTS

Work at Yonsei University was supported by National Research Foundation (NRF) grants funded by the Korean Government (MSIT; grant 2021R1A2C3004989, 2020R1A2C3013673) and the SRC program (vdWMRC; grant 2017R1A5A1014862). Computational resources were provided by the KISTI Supercomputing Center (project no. KSC-2022-CRE-0266). Work at Seoul National University was supported by the Leading Researcher Program (grant 2020R1A3B2079375) of the NRF of Korea.

ABBREVIATIONS

vdW, van der Waals; DFT, density-functional theory; IR, infrared

REFERENCES

(1) Novoselov, K. S.; Geim, A. K.; Morozov, S. V.; Jiang, D.; Zhang, Y.; Dubonos, S. V.; Grigorieva, I. V.; Firsov, A. A. Electric field effect in atomically thin carbon films. *Science* **2004**, *306*, 666−669.

(2) Li, L. K.; Yu, Y. J.; Ye, G. J.; Ge, Q. Q.; Ou, X. D.; Wu, H.; Feng, D. L.; Chen, X. H.; Zhang, Y. B. Black phosphorus field-effect transistors. *Nat. Nanotechnol.* **2014**, *9*, 372−377.

(3) Wang, Q. H.; Kalantar-Zadeh, K.; Kis, A.; Coleman, J. N.; Strano, M. S. Electronics and optoelectronics of two-dimensional transition metal dichalcogenides. *Nat. Nanotechnol.* **2012**, *7*, 699−712.

(4) Watanabe, K.; Taniguchi, T.; Kanda, H. Direct-bandgap properties and evidence for ultraviolet lasing of hexagonal boron nitride single crystal. *Nat. Mater.* **2004**, *3*, 404−409.

(5) Mak, K. F.; He, K. L.; Shan, J.; Heinz, T. F. Control of valley polarization in monolayer MoS_2 by optical helicity. *Nat. Nanotechnol.* **2012**, *7*, 494−498.

(6) Tang, S. J.; Zhang, C. F.; Wong, D.; Pedramrazi, Z.; Tsai, H. Z.; Jia, C. J.; Moritz, B.; Claassen, M.; Ryu, H.; Kahn, S.; Jiang, J.; Yan, H.; Hashimoto, M.; Lu, D. H.; Moore, R. G.; Hwang, C. C.; Hwang, C.; Hussain, Z.; Chen, Y. L.; Ugeda, M. M.; Liu, Z.; Xie, X. M.; Devereaux, T. P.; Crommie, M. F.; Mo, S. K.; Shen, Z. X. Quantum spin Hall state in monolayer 1T′-WTe_2. *Nat. Phys.* **2017**, *13*, 683−687.

(7) Georgi, A.; Nemes-Incze, P.; Carrillo-Bastos, R.; Faria, D.; Viola Kusminskiy, S.; Zhai, D. W.; Schneider, M.; Subramaniam, D.; Mashoff, T.; Freitag, N. M.; Liebmann, M.; Pratzer, M.; Wirtz, L.; Woods, C. R.; Gorbachev, R. V.; Cao, Y.; Novoselov, K. S.; Sandler, N.; Morgenstern, M. Tuning the Pseudospin Polarization of Graphene by a Pseudomagnetic Field. *Nano Lett.* **2017**, *17*, 2240−2245.

(8) Bonilla, M.; Kolekar, S.; Ma, Y. J.; Diaz, H. C.; Kalappattil, V.; Das, R.; Eggers, T.; Gutierrez, H. R.; Phan, M. H.; Batzill, M. Strong room-temperature ferromagnetism in VSe_2 monolayers on van der Waals substrates. *Nat. Nanotechnol.* **2018**, *13*, 289−293.

(9) Huang, B.; Clark, G.; Klein, D. R.; MacNeill, D.; Navarro-Moratalla, E.; Seyler, K. L.; Wilson, N.; McGuire, M. A.; Cobden, D. H.; Xiao, D.; Yao, W.; Jarillo-Herrero, P.; Xu, X. D. Electrical control of 2D magnetism in bilayer CrI_3. *Nat. Nanotechnol.* **2018**, *13*, 544−548.

(10) Gong, C.; Li, L.; Li, Z. L.; Ji, H. W.; Stern, A.; Xia, Y.; Cao, T.; Bao, W.; Wang, C. Z.; Wang, Y. A.; Qiu, Z. Q.; Cava, R. J.; Louie, S. G.; Xia, J.; Zhang, X. Discovery of intrinsic ferromagnetism in two-dimensional van der Waals crystals. *Nature* **2017**, *546*, 265−269.

(11) Fei, Z. Y.; Huang, B.; Malinowski, P.; Wang, W. B.; Song, T. C.; Sanchez, J.; Yao, W.; Xiao, D.; Zhu, X. Y.; May, A. F.; Wu, W. D.; Cobden, D. H.; Chu, J. H.; Xu, X. D. Two-dimensional itinerant ferromagnetism in atomically thin Fe_3GeTe_2. *Nat. Mater.* **2018**, *17*, 778−782.

(12) Kang, S.; Kim, K.; Kim, B. H.; Kim, J.; Sim, K. I.; Lee, J. U.; Lee, S.; Park, K.; Yun, S.; Kim, T.; Nag, A.; Walters, A.; Garcia-Fernandez, M.; Li, J.; Chapon, L.; Zhou, K. J.; Son, Y. W.; Kim, J. H.; Cheong, H.; Park, J. G. Coherent many-body exciton in van der Waals antiferromagnet $NiPS_3$. *Nature* **2020**, *583*, 785−789.

(13) Lee, J. U.; Lee, S.; Ryoo, J. H.; Kang, S.; Kim, T. Y.; Kim, P.; Park, C. H.; Park, J. G.; Cheong, H. Ising-Type Magnetic Ordering in Atomically Thin $FePS_3$. *Nano Lett.* **2016**, *16*, 7433−7438.

(14) Haraguchi, Y.; Michioka, C.; Ishikawa, M.; Nakano, Y.; Yamochi, H.; Ueda, H.; Yoshimura, K. Magnetic Nonmagnetic Phase Transition with Interlayer Charge Disproportionation of Nb-3 Trimers in the Cluster Compound Nb_3CI_8. *Inorg. Chem.* **2017**, *56*, 3483−3488.

(15) Sheckelton, J. P.; Plumb, K. W.; Trump, B. A.; Broholm, C. L.; McQueen, T. M. Rearrangement of van der Waals stacking and formation of a singlet state at T=90 K in a cluster magnet. *Inorg. Chem. Front.* **2017**, *4*, 481−490.

(16) Pasco, C. M.; El Baggari, I.; Bianco, E.; Kourkoutis, L. F.; McQueen, T. M. Tunable Magnetic Transition to a Singlet Ground State in a 2D van der Waals Layered Trimerized Kagome Magnet. *ACS Nano* **2019**, *13*, 9457−9463.

(17) Jiang, J. K.; Liang, Q. H.; Meng, R. S.; Yang, Q.; Tan, C. J.; Sun, X.; Chen, X. P. Exploration of new ferromagnetic, semiconducting and biocompatible Nb_3X_8 (X = Cl, Br or I) monolayers with considerable visible and infrared light absorption. *Nanoscale* **2017**, *9*, 2992−3001.

(18) Sun, Z. Y.; Zhou, H.; Wang, C. X.; Kumar, S.; Geng, D. Y.; Yue, S. S.; Han, X.; Haraguchi, Y.; Shimada, K.; Cheng, P.; Chen, L.; Shi, Y. G.; Wu, K. H.; Meng, S.; Feng, B. J. Observation of Topological Flat Bands in the Kagome Semiconductor Nb_3Cl_8. *Nano Lett.* **2022**, *22*, 4596−4602.

(19) Oh, S.; Choi, K. H.; Chae, S.; Kim, B. J.; Jeong, B. J.; Lee, S. H.; Jeon, J.; Kim, Y.; Nanda, S. S.; Shi, L.; Yi, D. K.; Lee, J. H.; Yu, H. K.; Choi, J. Y. Large-area synthesis of van der Waals two-dimensional material Nb_3I_8 and its infrared detection applications. *J. Alloys Compd.* **2020**, *831*, 154877.

(20) Regmi, S.; Fernando, T. W.; Zhao, Y.; Sakhya, A. P.; Dhakal, G.; Elius, I. B.; Vazquez, H.; Denlinger, J. D.; Yang, J.; Chu, J.-H., Spectroscopic evidence of flat bands in breathing kagome semiconductor Nb_3I_8. **2022**, arXiv:2203.10547. arXiv preprint.

(21) Giannozzi, P.; Baroni, S.; Bonini, N.; Calandra, M.; Car, R.; Cavazzoni, C.; Ceresoli, D.; Chiarotti, G. L.; Cococcioni, M.; Dabo, I.; Dal Corso, A.; de Gironcoli, S.; Fabris, S.; Fratesi, G.; Gebauer, R.; Gerstmann, U.; Gougoussis, C.; Kokalj, A.; Lazzeri, M.; Martin-Samos, L.; Marzari, N.; Mauri, F.; Mazzarello, R.; Paolini, S.; Pasquarello, A.; Paulatto, L.; Sbraccia, C.; Scandolo, S.; Sclauzero, G.; Seitsonen, A. P.; Smogunov, A.; Umari, P.; Wentzcovitch, R. M. QUANTUM ESPRESSO: a modular and open-source software project for quantum simulations of materials. *J. Phys.: Condens. Matter* **2009**, *21*, 395502.

(22) van Setten, M. J.; Giantomassi, M.; Bousquet, E.; Verstraete, M. J.; Hamann, D. R.; Gonze, X.; Rignanese, G. M. The PSEUDODOJO: Training and grading a 85 element optimized norm-conserving pseudopotential table. *Comput. Phys. Commun.* **2018**, *226*, 39−54.

(23) Sabatini, R.; Gorni, T.; de Gironcoli, S. Nonlocal van der Waals density functional made simple and efficient. *Phys. Rev. B: Condens. Matter Mater. Phys.* **2013**, *87*, 041108.

(24) Baroni, S.; de Gironcoli, S.; Dal Corso, A.; Giannozzi, P. Phonons and related crystal properties from density-functional perturbation theory. *Rev. Mod. Phys.* **2001**, *73*, 515−562.

(25) Hulliger, F. *Structural Chemistry of Layer-Type Phases*; Springer Science & Business Media, 1976.

(26) Magonov, S. N.; Zoennchen, P.; Rotter, H.; Cantow, H. J.; Thiele, G.; Ren, J.; Whangbo, M. H. Scanning tunneling and atomic force microscopy study of layered transition-metal halides Nb_3X_8 (X = Cl, Br, I). *J. Am. Chem. Soc.* **1993**, *115*, 2495−2503.

(27) Simon, A.; Von Schnering, H. G. β-Nb_3Br_8 und β-Nb_3J_8 darstellung, eigenschaften und struktur. *J. Less-Common Met.* **1966**, *11*, 31−46.

https://doi.org/10.1021/acsomega.3c01019
ACS Omega 2023, 8, 14190−14196